Design and Performance Analysis of a Bioelectronic Controlled Hybrid Serial-Parallel Wrist Exoskeleton

Xueze Zhang, Minjie Wang, Hongbo Wang, *Member, IEEE*, Fuhao Wang, *Graduate Student Member, IEEE*, Li Chen, Wei Mu, Junkongshuai Wang, and Xiaoyang Kang, *Member, IEEE*

***Abstract*— Wrist exoskeletons are increasingly being used in the rehabilitation of stroke and hand dysfunction because of its ability to assist patients in high intensity, repetitive, targeted and interactive rehabilitation training. However, the existing wrist exoskeletons cannot effectively replace the work of therapist and improve hand function, mainly because the existing exoskeletons cannot assist patients to perform natural hand movement covering the entire physiological motor space (PMS). Here, we present a bioelectronic controlled hybrid serial-parallel wrist exoskeleton HrWr-ExoSkeleton (HrWE) which is based on the PMS design guidance, the gear set can carry out forearm pronation/supination (P/S) and the 2-DoF parallel configuration fixed on the gear set can carry out wrist flexion/extension (F/E) and radial/ulnar deviation (R/U). This special configuration not only provides enough range of motion (RoM) for rehabilitation training (85F/85E, 55R/55U, and 90P/90S), but also makes it easier to provide the interface for finger exoskeletons and be adapted to upper limb exoskeletons. In addition, to further improve the rehabilitation effect, we propose a HrWE-assisted active rehabilitation training platform based on surface electromyography signals.**

***Index Terms*— Wrist exoskeleton, active rehabilitation, wrist rehabilitation, mechanical design.**

Manuscript received 29 November 2022; revised 5 May 2023; accepted 3 June 2023. Date of publication 7 June 2023; date of current version 14 June 2023. This work was supported in part by the National Key Research and Development Program of China under Grant 2021YFC0122700; in part by the National Natural Science Foundation of China under Grant 61904038 and Grant U1913216; in part by the Shanghai Sailing Program under Grant 19YF1403600; in part by the Shanghai Municipal Science and Technology Commission under Grant 19441907600; in part by the Opening Project of Zhejiang Laboratory under Grant 2021MC0AB01; in part by the Fudan University-Changchun Institute of Optics, Fine Mechanics and Physics (CIOMP) Joint Fund under Grant FC2019-002; in part by the Ji Hua Laboratory under Grant X190021TB190 and Grant X190021TB193; in part by the Shanghai Municipal Science and Technology Major Project under Grant 2021SHZDZX0103 and Grant 2018SHZDZX01; in part by the Zhang Jiang (ZJ) Laboratory; and in part by the Shanghai Center for Brain Science and Brain-Inspired Technology. *(Corresponding author: Xiaoyang Kang.)*

This work involved human subjects or animals in its research. Approval of all ethical and experimental procedures and protocols was granted by the Ethics Committee of FUDAN University and Xi'an Jiaotong University under Application No. 2019-776, and performed in line with the Declaration of Helsinki.

Xueze Zhang, Minjie Wang, Fuhao Wang, Li Chen, Wei Mu, and Junkongshuai Wang are with the Laboratory for Neural Interface and Brain Computer Interface, the State Key Laboratory of Medical Neurobiology, the Engineering Research Center of AI and Robotics, Ministry of Education, the Shanghai Engineering Research Center of AI and Robotics, the MOE Frontiers Center for Brain Science, Institute of AI and Robotics, and the Institute of Meta-Medical, Academy for Engineering and Technology, Fudan University, Shanghai 200433, China.

Hongbo Wang is with the with the Laboratory for Neural Interface and Brain Computer Interface, the State Key Laboratory of Medical Neurobiology, the Engineering Research Center of AI and Robotics, Ministry of Education, the Shanghai Engineering Research Center of AI and Robotics, the MOE Frontiers Center for Brain Science, Institute of AI and Robotics, and the Institute of Meta-Medical, Academy for Engineering and Technology, Fudan University, Shanghai 200433, China, and also with the School of Life Science and Technology, Xi'an Jiaotong University, Xi'an, Shaanxi 710049, China.

Xiaoyang Kang is with the Laboratory for Neural Interface and Brain Computer Interface, the State Key Laboratory of Medical Neurobiology, the Engineering Research Center of AI and Robotics, Ministry of Education, the Shanghai Engineering Research Center of AI and Robotics, the MOE Frontiers Center for Brain Science, Institute of AI and Robotics, and the Institute of Meta-Medical, Academy for Engineering and Technology, Fudan University, Shanghai 200433, China, also with the Yiwu Research Institute, Fudan University, Yiwu, Zhejiang 322000, China, also with the Ji Hua Laboratory, Foshan, Guangdong 528200, China, and also with the Research Center for Intelligent Sensing Zhejiang Laboratory, Hangzhou 311121, China (e-mail: xiaoyang_kang@fudan.edu.cn).

Digital Object Identifier 10.1109/TNSRE.2023.3283603

NOMENCLATURE

R :	Rotational joint.
S :	Spherical joint.
F :	Degree of freedom (DoF).
F/E:	flexion/extension.
R/U:	Radial/ulnar deviation.
P/S:	Pronation/supination.
n :	Number of links.
p :	Number of joints.
fi :	DoF of each joint.
f :	Local DoF.
z_i :	Axis of joint i in each SOC.
x_i :	Normal direction between adjacent axes in each SOC.
a_i :	The distance between z_i and z_{i+1}.
d_i :	The distance between x_i and x_{i+1}.
l_i :	Length of i-th link.
γ_i^j :	Rotation angle around x_i^j.
θ_i^j :	Rotation angle around z_i^j.
C_i :	Coordinates of the rotation axes in the $\{i\}$.
A_i :	Normal direction between adjacent axes in each SOC.
T_i :	Rotation transformation matrix in each SOC.
H_i :	Position vector of joints in each SOC.
P_i :	Position vector of point in coordinate.
P :	Position vector of point in $\{0\}$.

q_i : Active angle.
α : Attitude angle of F/E joint.
β : Attitude angle of R/U joint.
$\dot{q_i}$: Velocity vector of active joint.
$\dot{\alpha}$: Velocity vector of α.
$\dot{\beta}$: Velocity vector of β.
J : Jacobian matrix.
κ : The condition number of 2-RSS/RR.

I. Introduction

STROKE causes a variety of neurological impairment in patients, and influences their ability of activities of daily living (ADL), which is a major factor leading to impaired hand function [1]. Rotary movements of the hand are important for manipulating objects: forearm pronation/supination (P/S), wrist flexion/extension (F/E) and wrist radial/ulnar deviation (R/U). Those behaviors are achieved by our specific muscles that produce target torque to corresponding joints. The conventional therapeutic for hand functional rehabilitation needs a long course of treatment and limited effectiveness [2]. In order to improve the rehabilitation effect, more and more scholars began to study the rehabilitation therapies based on robotic strategies [3]. Although many literatures show that robot-assisted rehabilitation strategies cannot improve the rehabilitation effects compared with the traditional rehabilitation strategies [4], [5], [6], the rehabilitation robots have the characteristics of low labor cost, simple operation and high efficiency [7], which is highly valued by clinicians and favored by patients.

Preliminary research indicates that upper limb exoskeletons, such as MIT-MANUS [8], [9], which is mainly focused on the proximal joints and the effect on the distal limb segments is limited [10]. Targeted adjuvant therapy for the lesion area can effectively improve the patient's ADL and motor function after stroke [11], [12]. To better stretch muscles, a lot of rehabilitation therapies of hand function restoration require the coordinated movement of the upper limb, fingers and wrist. For example, in the upper limb tension test (ULTT), the therapist assists the patient perform synergistic movements of upper limb, wrist and fingers [13], [14], [15]. In addition, the exoskeleton designed based on PMS is more conducive to the development of robot-assisted hand rehabilitation therapy and the revelation of rehabilitation mechanism [16]. Therefore, when designing wrist exoskeleton, we should consider not only its workspace, but also how to combine it with upper limb exoskeleton and finger exoskeleton.

The special configuration of wrist reduces the wrist joint to a spherical joint and require the axes of each motion to intersect at one point, which represents a challenge for the mechanical design of wrist exoskeletons [17], [18], [19]. In recent years, several exoskeletons for wrist rehabilitation have been presented (see Table I). Existing wrist exoskeletons based on series structure design can provide interfaces for hand function rehabilitation modules and be modified into upper limb rehabilitation robots. For example, the finger-wrist collaborative rehabilitation exoskeleton developed by Ueki et al. [20] has 18-DoF, and its biggest characteristic is that each of the four fingers has 1-DoF of adduction/abduction. The upper limb exoskeleton WRES developed by Buongiorno et al. has 8-DoF and can achieve the synergistic rehabilitation of upper limb, wrist and fingers [21]. However, due to the characteristics of the series structure, there will be interference between the connecting rods, which leads to the limitation of the workspace [21], [22], [23], [24]. Besides, most of the parallel-based wrist exoskeletons are also restricted by workspace [25], [26]. WG provides sufficient workspace [27], but its large size makes it difficult to be modified into upper limb rehabilitation robots. PWRR provides sufficient workspace in FE and RU joints, but it lacks DoF in the axis of P/S [28].

To solve these problems, a novel 3-DoF wrist exoskeleton HrWrist ExoSkeleton (HrWE) based on hybrid series-parallel

TABLE I
Capability Analysis of HrWE and Other External Wrist Exoskeletons

Device	Range of motion (deg)		
	P/S	F/E	R/U
Wrist [25]	157 (71P/86S)	144 (73F/71E)	52 (19R/33U)
WRES [21]	146	75	40
WR [22]	160 (80P/80S)	144 (72F/72E)	72 (27R/45U)
RW-S [23]	180	130	75
OW [24]	170 (85P/85S)	135 (70/65)	75 (35/40)
RW [25]	180 (90P/90S)	84 (42F/42E)	52 (19R/33U)
PAM-Wr [26]	161 (88P/73S)	148 (75F/73E)	53 (19R/34U)
WG [27]	180	180	160
PWRR [28]	/	130 (65F/65E)	105 (25R/80U)
HrWE	180 (90P/90S)	170 (85F/85E))	110 (55R/55U)

TABLE II
The Parameters of Each SOC

d	a	γ	θ
$SOC1$			
0	l_2	0°	$-90° + \theta_1^1$
0	0	90°	θ_2^1
0	l_1	0°	$180° + \theta_3^1$
0	0	90°	θ_4^1
$SOC2$			
0	l_2	0°	$-90° + \theta_1^2$
0	0	90°	θ_2^2
0	l_1	0°	$180° + \theta_3^2$
0	0	90°	θ_4^2
$SOC3$			
l_2	0	90°	θ_3^3

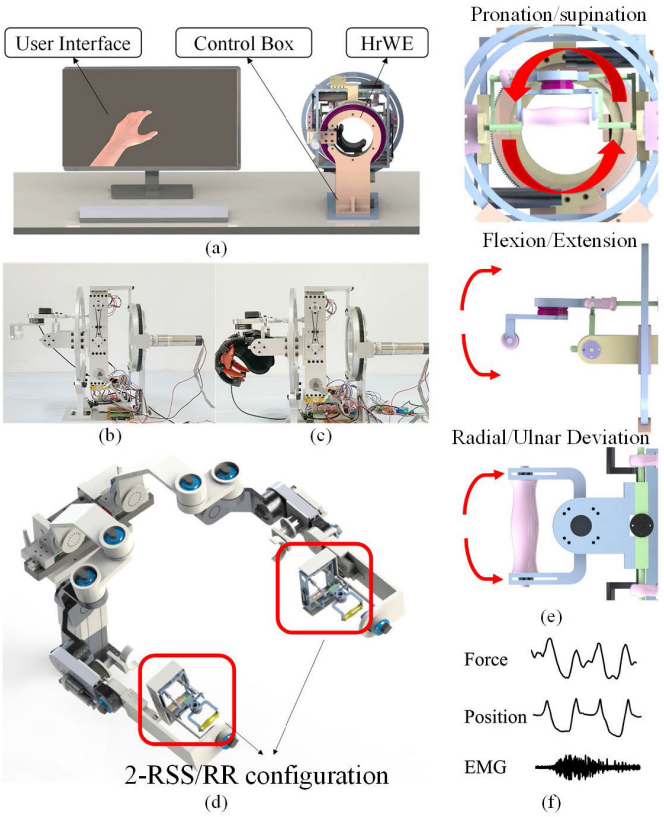

Fig. 1. (a) The hand function rehabilitation system overview. The system consists of the HrWE, control box and human-machine interface. (b)-(d) The modifiability of HrWE. The end-effector of the HrWE can be attached to a handle or an exoglove, and the 2-RSS/RR configuration can be adapted to the upper limb exoskeleton. (e) The manipulability of HrWE. HrWE can assist wrist to perform F/E, R/U and P/S movements, and it is suit for both hands. (f) The multimodal features recording ability. The HrWE can record kinematic features, force and muscle activities.

configuration is proposed in this paper (see Fig. 1(a)). In HrWE, a gear set is used to drive the P/S joint, and a 2-DoF parallel mechanism 2-RSS/RR mounted on the gear set is used to drive the F/E and R/U joints, where R represents the revolute joint and S represent the spherical joint. Moreover, we design a sEMG based active rehabilitation platform. The overview of HrWE is shown in Fig. 1, and it has the following advantages:

1) Modifiable. The end-effector of HrWE can be fitted with the handle or exoglove (see Fig. 1(b)-(c)). With simple modifications, the HrWE structure can be modified to the upper limb exoskeleton (see Fig. 1(d)).
2) Manipulability. HrWE can assist users to perform P/S, F/E and R/U movements (see Fig. 1(e)), and the workspace of HrWE can fully encircle the PMS of wrist (see Table I). This advantage can better stretch the wrist muscles. Moreover, HrWE is versatile in both hands and suitable for most individuals.

The rest of this paper is organized as follows: Section II is the design overview of HrWE; In section III, we analyze the kinematic performance of HrWE; Section IV introduces the active rehabilitation training platform we set up, In Section V, we fully discuss strengths and weaknesses of HrWE; Section VI summarizes and anticipates the current work.

II. Mechanical Design and Kinematic Analysis of HrWE

A. Requirement

The wrist exoskeleton can be used for rehabilitation training of most hand functional injures except for extreme cases such as fracture, unstable joint, and trauma. In order to reduce stress on therapists and provide more standardized rehabilitation training, rehabilitation robots should replace therapists as much as possible, which puts higher requirements on wrist exoskeletons.

The first key requirement is that the wrist exoskeleton should assist execution of standardized, highly repeatable specified movements [29]. The wrist exoskeleton needs to provide 3-DoF of wrist movements and should provide enough torque to the corresponding axes (0.06Nm for P/S, 0.35Nm for F/E and 0.35Nm for R/U) [21]. In addition, the wrist exoskeletons should be appropriate for both left and right hands.

The second key requirement is that the wrist exoskeleton's RoM should encircle the PMS of wrist, provide the interface for the finger exoskeleton module and can be modified into the upper limb exoskeletons easily. Those characteristics allow the upper limb exoskeletons to assist patient's wrist covering the PMS with the arm and fingers to be stretched simultaneously, like ULTT.

The third key requirement is that the wrist exoskeleton should provide active rehabilitation paradigm. Clinical studies indicate that robot-assisted rehabilitation training cannot effectively promote neural circuit remodeling [30], [31]. This is because the recovery and reconstruction of nerve function largely depends on active rehabilitation training treatment [16], [32], which requires that the rehabilitation training platform can recognize users' movement intentions.

The fourth key requirement is to record kinematic features, multidimensional force and muscle activities. The kinematic features and multidimensional force are crucial to control the wrist exoskeletons. The real-time multiple modalities information feedback helps to recognize the movement intentions, adjust the intensity of rehabilitation training and improve patients' positivity during convalescent period.

The fifth requirement involves the human-computer interaction performance. Factors that affect the user experience, such as weight, volume, portability and operability, need to be considered in the design process.

B. Design of the HrWE

We propose a novel 3-DoF wrist exoskeleton HrWE (see Fig. 2(a)), which meets the design requirements. The HrWE can actuate P/S, F/E and R/U joints individually or simultaneously.

The mechanical configuration of HrWE consists of a base, a 2-DoF parallel configuration 2-RSS/RR used to actuate F/E and R/U joints (see Fig. 2(b)) and a revolute joint used to actuate P/S joint (see Fig. 2(c)). The drive line of P/S joint

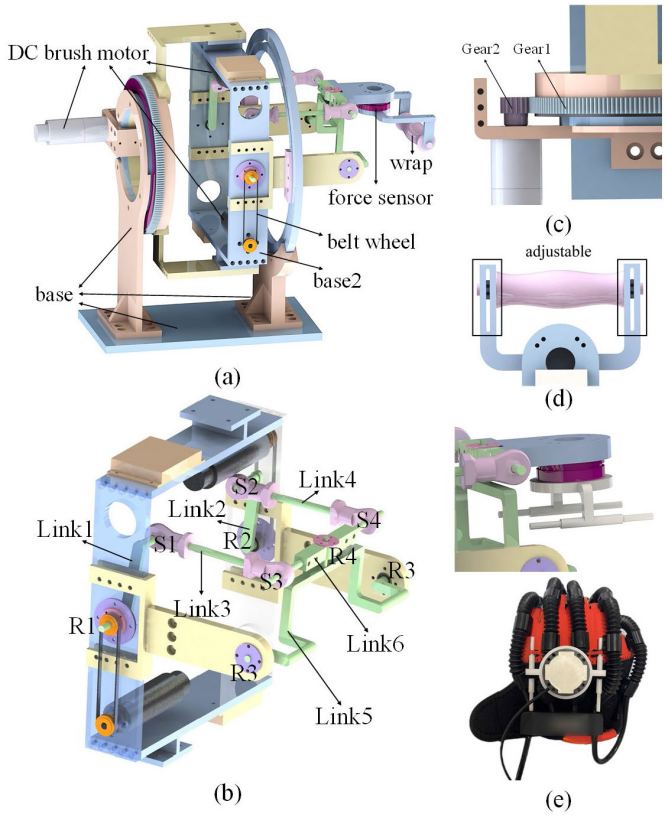

Fig. 2. (a) The CAD model of HrWE; (b) the 2-DoF parallel configuration 2-RSS/RR used to actuate F/E and R/U joints. (c) the configuration used to actuate P/S joint; (d) the handle; (e) the connection interface between HrWE and exoglove.

consists of a DC motor (SR308524B-P32H-320.01, nominal torque: 85.6 mNm, 24V, SMJ., China) and a gear set. The gear set has a transmission ratio of 1:11.76. The 2-DoF parallel configuration 2-RSS/RR is fixed to the P/S drive configuration through a connection frame *base2*. Different from the PWRR configuration proposed in [28], the 2-RSS/RR configuration is driven by gear motors, and all joints of the mechanism are revolute joints. Compared to the pneumatic system, electric system has the advantages of higher control accuracy, lower noise and smaller mechanism size.

In the 2-RSS/RR configuration, two RSS branches are used to drive F/E and R/U joints independently or simultaneously. Two identical DC brush motors (SR235824B-01-P28H-200.2, nominal torque: 28.1mNm, 24V, SMJ, China) are used to drive *R1* and *R2* respectively. To optimize the mechanism space, the DC brush motors are mounted on *base2* and drive joints *R1* and *R2* through the belt wheel. Taking into account the size of human arm (arm length: 64∼89cm [33], wrist circumference: 14∼22cm [34], and palm length: 8∼12cm [35]), configuration performance and mechanism size, the distance between *S1* and *S2* is set as 130 mm, the distance between *S3* and *S4* is set as 130mm, the length of *Link1* and *Link2* is set as 65mm, and the length of *Link3* and *Link4* is set as 130mm. *R3* and *R4* are the passive joints, and the attitude angles $\alpha_{\mathrm{F/E}}\alpha_{\mathrm{F/E}}$ and $\beta_{R/U}\beta_{\mathrm{R/U}}$ are equal to the rotation angles of F/E and R/U joints. Based on the principle of ergonomics, *Link5* adopts a special-shaped configuration to provide placement area for hand and prevent interference (suitable for individuals with wrist circumference less than 30cm). *Link6* can revolute around axis of R/U.

When using HrWE for wrist rehabilitation training, the hand and arm must be fixed to the device. In order to improve the user experience, we fix a sponge on the inner wall of the big gear. Comprehensive consideration of user comfort and compact configuration, the *Gear1* is perforated with an 80mm diameter through hole and the bracket is placed inside the hole. During rehabilitation training, the patient is asked to place the forearm on the sponge and hold the handle (see Fig. 1(b)), or the hand is fixed on the exoglove (Yisheng C10, SIYI INTELLIGENCE, China, see Fig. 1(c)). The position of the grip is adjustable in the direction of the arm (see Fig. 2(d)), which aligns the center of the wrist with the HrWE center of rotation for different individuals (palm length from 8cm to 12cm). The exoglove is fixed to HrWE through the connection intrerface (see Fig. 2(e)). A three-dimensional force sensor (ZKMD3D310, HUMANETICS, China) was installed at the end of HrWE (see Fig. 2(a)).

The whole HrWE includes mechanical configuration part, control system part and user interaction part. The mechanical configuration is described in detail above, and the control system adopts PID strategy which supported by motor control unit (MOSVO, China). Before wrist rehabilitation training, it is necessary to input the patient's pain threshold, PMS of wrist and intensity of rehabilitation training (training time and movement speed) to prevent the patient from secondary injury. In an emergency, both the therapists and the patients can use the emergency stop button to turn off the power of the system. The human-computer interaction interface is developed based on Unity (Unity Technologies, USA). During rehabilitation training, the subjects are required to follow the same movements based on the screen and voice prompts. Such visual and auditory feedback can help to maintain the patient's high attention throughout the rehabilitation process and more conducive to neurological recovery [32].

C. Kinematics of the HrWE

The kinematic performance of P/S joint is determined by the characteristics of the revolute joint *R0* (i.e. *Gear1*), and the RoM of P/S is ±90°. In the rest part of this chapter, we will focus on analyzing the kinematic characteristics of 2-RSS/RR.

The basic configuration of 2-RSS/RR is shown in Fig. 3(a). According to (1), the mechanism is a 2-DoF parallel configuration. Where n denotes the number of links, p denotes the number of joints, fi denotes the DoF of each joint, and f denotes the local DoF. In order to establish 2-RSS/RR kinematic model, multiple coordinate systems must be established. As shown in Fig. 3(a), *R1* and *R2* are active joints of 2-RSS/RR, while the performance of *R3* and *R4* determines the attitude angle $\alpha_{\mathrm{F/E}}$ and $\beta_{R/U}$.

$$F = 6(n-p) + \sum_{i=1}^{p} fi - f = 2 \tag{1}$$

According to the above analysis, there are local DoF at *Link3* and *Link4*, so the spherical joints *S1*, *S2*, *S3* and *S4* can be simplified as universal joints. A static coordinate system 0 is set at the virtual center of *R1* and *R2*, where x_0 is parallel to

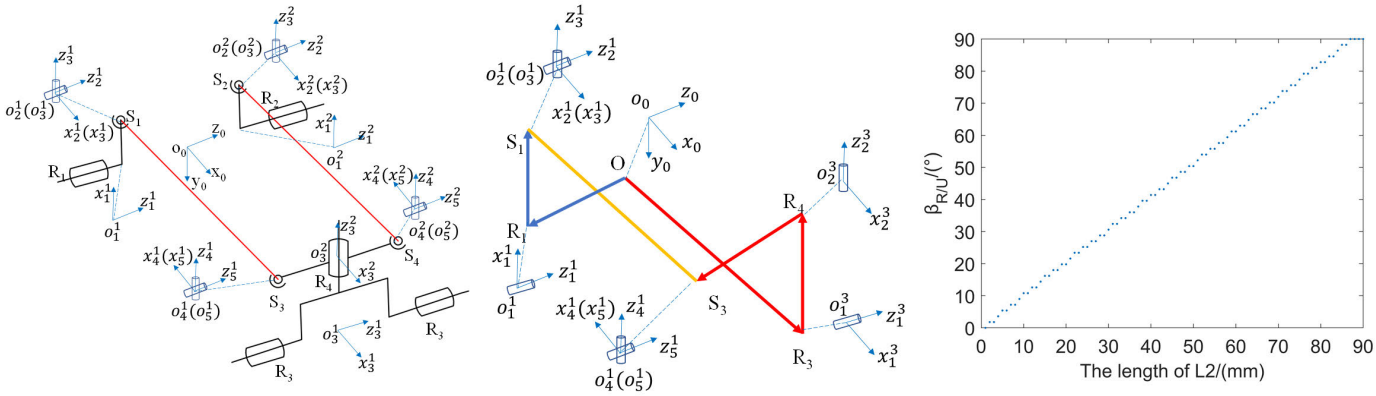

Fig. 3. (a) Schematic diagram of 2-RSS/RR where R1 and R2 are the active joints. The coordinates of each joint are established based on the screw theory and there are three single-open chains in this configuration: R1-S1-S3, R2-S2-S4 and R3-R4. (b) The closed vector loop of the drive branch RSSR. (c) The relationship between the drive link and the kinematics of R/U movement.

the rotation axis of F/E joint, y_0 is parallel to the rotation axis of P/S joint, and z_0 is parallel to the rotation axis of R/U joint. In order to easily describe the characteristics of 2-RSS/RR, a screw coordinate system is established, where z_i represents the rotation axis of the joint, x_i is the common normal line of z_i and z_{i+1}, the origin i of the coordinate system is at the center of the rotation axis i, a_i is the distance between z_i and z_{i+1}, and d_i is the distance between x_i and x_{i+1}.

The single-open chain (SOC) analysis method [36] is used to analysis the kinematic performance of the 2-RSS/RR configuration. 2-RSS/RR consists of three SOCs (SOC1: *R1-S1-S3*, SOC2: *R2-S2-S4*, SOC3: *R3-R4*) and the end-effector (*S3-S4*). We define that the coordinates of the rotation axes in the i coordinate system of chain j as the unit vector C_i^j, and define the normal direction between adjacent axes as the unit vector A_i^j. In each SOC, C_i and A_i can be expressed as (2) and (3) respectively.

$$C_i = \begin{cases} [0 \quad 0 \quad 1]^T & i = 1 \\ T_{i-1}\left[0 \quad -s\gamma_{i-1}c\gamma_{i-1}\right]^T & i > 1 \end{cases} \tag{2}$$

$$A_i = \begin{cases} [c\theta_i \quad s\theta_i \quad 0]^T & i = 1 \\ T_{i-1}\left[c\theta_i c\gamma_{i-1} s\theta_i s\gamma_{i-1} s\theta_i\right]^T & i > 1 \end{cases} \tag{3}$$

where s and c are the simple expression of sin and cos respectively. T_i represents the rotation transformation matrix between the link coordinate system and the fixed coordinate system direction, and T_i can be expressed as (4).

$$T_i = \left[A_i \;\; C_i \times A_i \;\; C_i \right] \tag{4}$$

In each SOC of the parallel mechanism, the coordinates of *i-th* joint in the first coordinate system 1} can be expressed as (5).

$$H_i = d_1C_1 + a_1A_1 + d_2C_2 + a_2A_2 \cdots + d_iC_i \tag{5}$$

The coordinates of any point P on *i-th* link in 1} can be expressed as (6).

$$P = H_i + T_i P_i \tag{6}$$

where P_i is the coordinate of point P in i.

In order to determine the RoM of the 2-RSS/RR configuration, the numerical solution method was used to solve the relationship between the attitude angle and active angle. The closed vector loop of the RSSR is constructed in Fig. 3(b). And the relationship between the active angle q_i and the attitude angle can be expressed by (7).

$$\begin{cases} l_1^2 = \left\| \overrightarrow{O_0S_3} - \overrightarrow{O_0S_1} \right\|^2 \\ l_1^2 = \left\| \overrightarrow{O_0S_4} - \overrightarrow{O_0S_2} \right\|^2 \end{cases} \tag{7}$$

where l_1 denotes the length of *Link3* and *Link4*. The position vectors $\overrightarrow{O_0S_1}$, $\overrightarrow{O_0S_2}$ can be calculated by (5), and $\overrightarrow{O_0S_3}$, $\overrightarrow{O_0S_4}$ can be calculated by (6). Each of them can be expressed as (8)-(11).

$$P_{s3} = \begin{bmatrix} l_2s\alpha + l_3c\alpha c\,(\beta - 90) + l_1 \\ l_3s\alpha c\,(\beta - 90) - l_2c\alpha \\ l_3s(\beta - 90) \end{bmatrix} \tag{8}$$

$$P_{s4} = \begin{bmatrix} l_2s\alpha + l_3c\alpha c\,(\beta + 90) + l_1 \\ l_3s\alpha c\,(\beta + 90) - l_2c\alpha \\ l_3s(\beta + 90) \end{bmatrix} \tag{9}$$

$$P_{s1} = \begin{bmatrix} l_2c(q_1 - 90) \\ l_2s(q_1 - 90) \\ -l_3 \end{bmatrix} \tag{10}$$

$$P_{s2} = \begin{bmatrix} l_2c(q_1 - 90) \\ l_2s(q_1 - 90) \\ l_3 \end{bmatrix} \tag{11}$$

where l_2 denotes the length of *Link1* and *Link2*, and l_3 denotes the half length of $\overrightarrow{S_1S_2}$ and $\overrightarrow{S_3S_4}$.

The derivative of (7) with respect to time t can be obtained as (12).

$$J_q \begin{bmatrix} \dot{q}_1 \\ \dot{q}_2 \end{bmatrix} - G \begin{bmatrix} \dot{\alpha} \\ \dot{\beta} \end{bmatrix} = 0 \tag{12}$$

where the matrices J_q and G are expressed as (13) and (14) respectively.

$$J_q = \begin{bmatrix} J_{q11} & 0 \\ 0 & J_{q12} \end{bmatrix} \tag{13}$$

$$G = \begin{bmatrix} G_{11} & G_{12} \\ G_{21} & G_{22} \end{bmatrix} \tag{14}$$

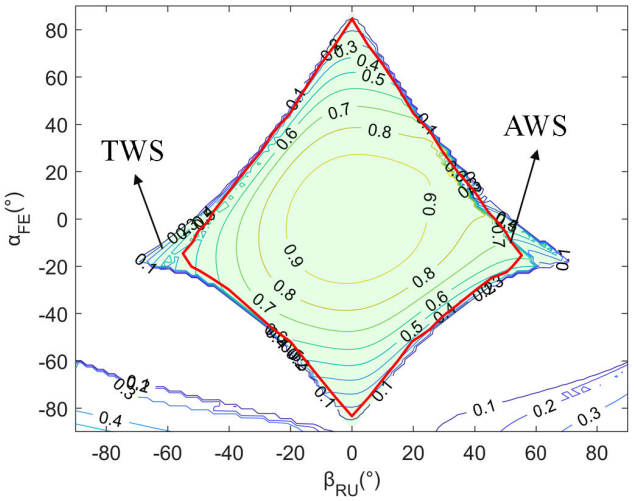

Fig. 4. Contours of condition number $1/\kappa$ in the TWS. The area within the red line is AWS of the 2-RSS/RR configuration.

If the matrix G is not singular, (12) can be expressed as (15).

$$\begin{bmatrix} \dot{\alpha} \\ \dot{\beta} \end{bmatrix} = J \begin{bmatrix} \dot{q_1} \\ \dot{q_2} \end{bmatrix} \tag{15}$$

where $J = G^{-1} J_q$ is the velocity Jacobian matrix.

According to the relationship between the velocity Jacobian matrix and the force Jacobian matrix, the relationship between the driving torque and the terminal output torque of the 2-RSS/RR mechanism can be expressed as (16).

$$\begin{bmatrix} \tau_{q_1} \\ \tau_{q_2} \end{bmatrix} = J^T \begin{bmatrix} \tau_\alpha \\ \tau_\beta \end{bmatrix} \tag{16}$$

where τ_α and τ_β are the torques of HrWE driving F/E and R/U, τ_{q_1} and τ_{q_2} are the output torque of the motors.

The kinematic characteristics of 2-RSS/RR are influenced by each link. In order to evaluate the effect of the 2-RSS/RR configuration on the expanding of R/U joint's RoM, we calculated the relationship between the drive link (*Link1* and *Link2*) and the extreme reach angle of R/U joint (The length of other links are fixed). As shown in Fig. 3(c), the longer length of the drive link, the larger RoM of R/U joint. In consideration of compact construction and terminal output torque, we sacrifice some RoM and set the length of *Link1* and *Link2* to 65mm. As shown in Fig. 2, the attitude angle $\gamma_{P/S}$ is not affected by the 2-RSS/RR configuration, and its kinematic characteristics are completely dependent on *Gear1*. Due to the configuration characteristics of 2-RSS/RR (see Fig. 3), *R1* and *R2* will reach the singularity of the configuration in the process of motion, and the attitude angle $\alpha_{F/E}$ and $\beta_{R/U}$ are jointly determined by *R1* and *R2*. Given the inputs of electrical actuators in joints *R1* and *R2*, the range of attitude angle $\alpha_{F/E}$ and $\beta_{R/U}$ can be solved by (7). The TWS is calculated and depicted in Fig. 4 and Fig. 5 ($-90^\circ < \alpha_{\mathrm{F/E}} < 90^\circ$, $-70.2^\circ < \beta_{\mathrm{R/U}} < 70.2^\circ$).

D. Condition Number Analysis

The condition number κ is an important index to judge the dexterity of mechanism, which defined as (17). When the condition number κ is equal to one, the mechanism reaches the isotropic point. On the contrary, when the condition number κ tends to infinity, the mechanism is close to singularity [37]. In order to ensure the manipulability of the mechanism, the condition number κ should be as close as possible to one.

$$\kappa = \|J\| \cdot \left\|J^{-1}\right\| \tag{17}$$

As can be seen from the Fig. 4, the change process of condition number is relatively gentle without abrupt peak, and the minimum value of κ is in the central region, and the value of κ increases gradually with the expansion of the region. $1/\kappa$ in the selected RoM region is greater than 0.2, indicating that HrWE has good manipulability.

III. Performance Analysis of HrWE

A. Workspace Analysis of 2-RSS/RR

The actual workspace (AWS) of HrWE is an important indicator to evaluate the performance of HrWE. We measured the AWS of the HrWE by an IMU (WT901C, WEITE Intelligent Technology, China) mounted at the end-effector. During the experiment, we defined the $\beta_{\mathrm{R/U}}$ with the step of 0.5° in the range of −70° to 70°, and found the corresponding value of $\alpha_{\mathrm{F/E}}$ at the TWS boundary according to $\beta_{\mathrm{R/U}}$. Then we get the active angles q_1 and q_2 by (7). Finally, we controlled the motor to reach the desired active angles q_1 and q_2, and recorded the attitude angles of HrWE from IMU as AWS ($-85.35^\circ < \alpha_{\mathrm{F/E}} < 85.44^\circ$, $-55.06^\circ < \beta_{\mathrm{R/U}} < 55.29^\circ$).

Although the PMS of the wrist is mentioned in reference [25], the actual PMS of the wrist varies from person to person. To verify that the AWS of 2-RSS/RR configuration can cover the PMS of the wrist, we designed an experiment to measure the PMS of the wrist. A group of four healthy volunteers were enrolled in this experiment. The participants consisted of two males (average age of 24, average height of 178cm, and average weight of 73.4kg) and two females (average age of 24, average height of 164cm, and average weight of 46.3kg).

The experimental platform predominantly consists of the Miqus M3 motion capture system (Qualisys, Inc., Gothenburg, Sweden), markers and custom armrest. The Miqus M3 motion capture system with six full view cameras is used to capture the 3D motion of the wrist, and the maximum shooting speed is up to 10000 fps when the field is narrowed down. As shown in Fig. 5, we designed a 3D printed base to define the reference coordinate system. M1 and M3 were symmetrically fixed to the sides of the 3D printed base, and M2 was fixed to the center of the top of the 3D printed base. The vector $\overrightarrow{M1M3}$ was defined as the axis of F/E joint and the vertical line of $\overrightarrow{M1M3}$ from M2 was defined as the axis of R/U joint. The axis of P/S joint is the common normal of the axes of F/E and R/U joints. A custom glove with markers was used to determine the hand orientation, the M4-M6 direction along the middle finger. The angle between the hand orientation and the axis of R/U was used to determine the rotation angle of F/E, and the angle between the hand orientation and the axis of F/E was used to determine the rotation angle of R/U. Before the experiment, the participants were asked to place their forearm on the experimental platform with their hand back up, and their

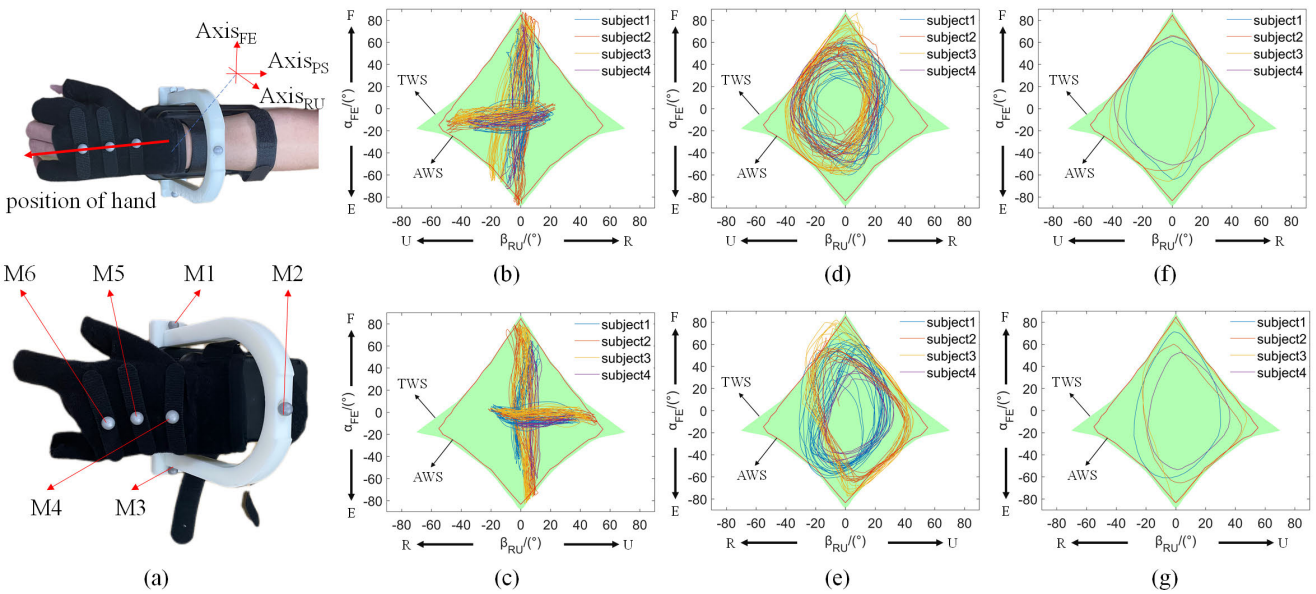

Fig. 5. (a) Experimental platform for measuring wrist PMS. M1-M6 are the six marks used to calculate the position of the wrist. (b) The PMS of left hand in the uniaxial task. (c) The PMS of right hand in the uniaxial task. (d) The PMS of left hand in the boundary elliptical movement task. (e) The PMS of right hand in the boundary elliptical movement task. (f) The PMS of left hand in the boundary elliptical movement task within device. (g) The PMS of left hand in the boundary elliptical movement task within device.

forearm was fixed on the experimental platform by straps to limit the movement of P/S joint. Each experiment consists of six sessions, and in each session, the participants were asked to repeat planned movements for 30 seconds. When the session was finished, participants were asked to relax their muscles. The collected first frame data was used to calibrate the deviation between the wrist's rotation axes and the reference coordinate axes.

The results are shown in Fig. 5(b)-(e), in boundary elliptical motion task, the AWS of HrWE can almost encircle the PMS of the wrist (out of AWS ratio: 0.049 ± 0.048). And in uniaxial motion task, the AWS of the HrWE is larger than the extreme position of the wrist ($-72.96 \pm 9.53° < \alpha_{F/E} < 77.17 \pm 6.92°$, $-41.63 \pm 7.78° < \beta_{R/U} < 43.26 \pm 9.53°$). To compare the achievable workspace within the device and outside the device for each subject, we controlled HrWE to assist subject reach the PMS position and use the IMU to record the reachable position of each subject. As the result is shown in Fig. 5(f)-(g), the workspace of the hand in the device is slightly less than the PMS (left hand inside/outside workspace area ratio: 95.59%, 102.55%, 94.40%, 107.32%; right hand inside/outside workspace area ratio: 87.07%, 96.79%, 84.51%, 109.04%; average ratio: $97.16 \pm 8.26\%$).

B. Kinematic Performance Analysis

Two different experiments have been performed to evaluate the kinematic performance of HrWE. The first experiment was aimed to tested whether 2-RSS/RR could provide standardized, highly repeatable specified movements. The second experiment was aimed to evaluate the torque output capability and the interaction torque monitoring capability. Due to the largest PMS in subject 3, subject 3 was invited to participate in these two experiments.

The trajectory tracking performance based on gear driven P/S motion has been demonstrated in [20] and [21], so the first

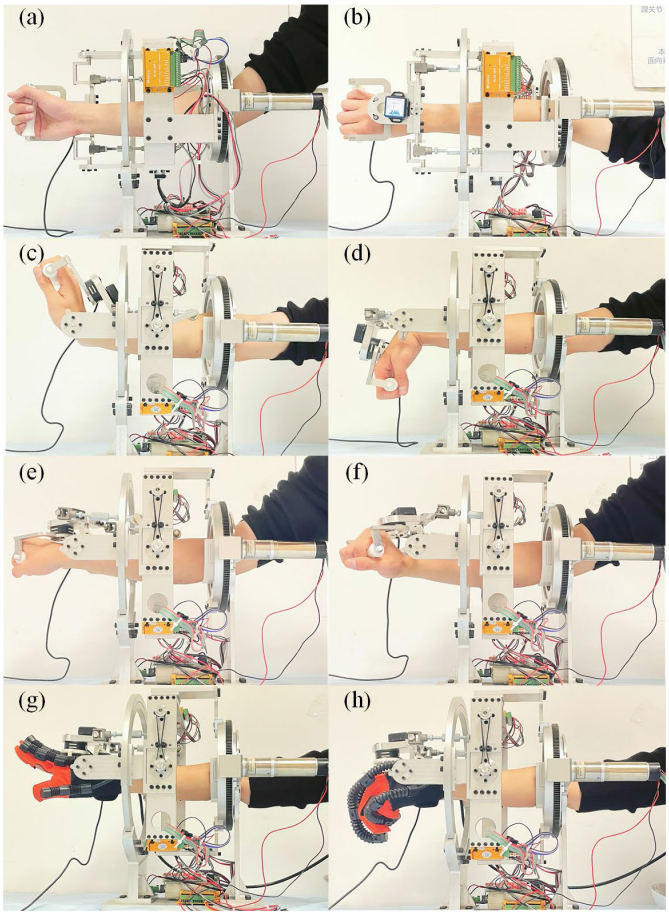

Fig. 6. HrWE under different tasks: (a) supination, (b) pronation, (c) extension, (d) flexion, (e) ulnar deviation, (f) radius deviation, (g) hand open, (h) hand close.

experiment only evaluated the trajectory tracking performance of 2-RSS/RR. In the first experiment, a program was set to control HrWE to assist subject 3 to perform standardized and

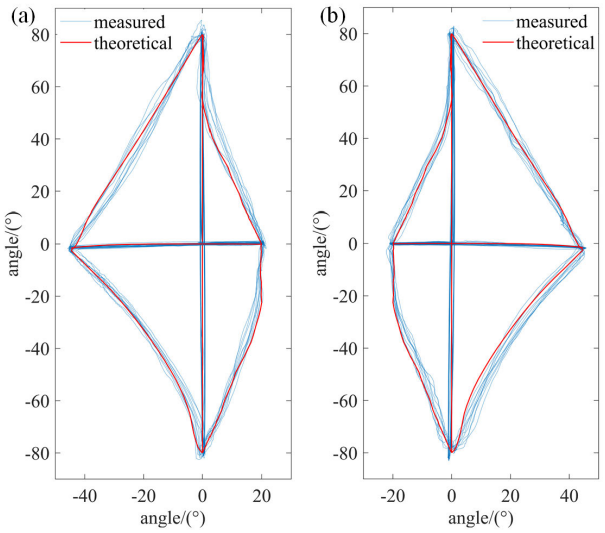

Fig. 7. The proposed trajectory (F/E, R/U and synergistic motion) tracking performance of HrWE on subject 3 during (a) left hand assisted movement and (b) right hand assisted movement.

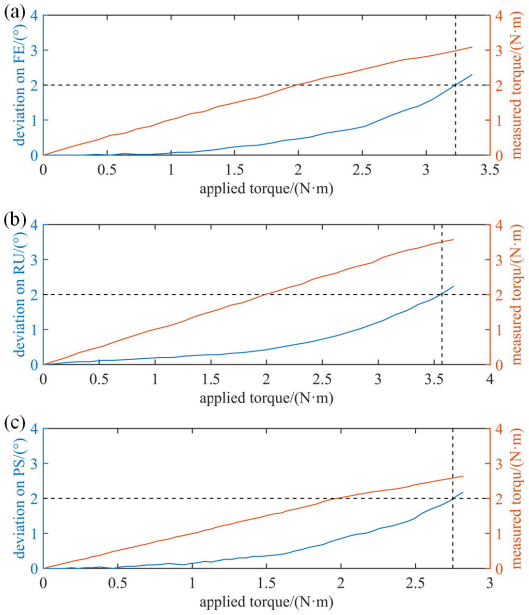

Fig. 8. HrWE torque output measurement and interactive force perception evaluation experiments in (a) F/E, (b) R/U and (c) P/S.

highly repeatable specified movements (F/E, R/U and synergistic motion). After starting the movement, encoder and IMU start collecting data simultaneously. Based on the data collected by the encoder, the theoretical trajectory of end-effector can be calculated through (7). The data measured by IMU is the actual trajectory of end-effector. Fig. 7 shows the trajectory tracking ability of HrWE assisted subject 3 during 10 times R/U, F/E, and synergistic motion in two different scenarios (left hand and right hand). The RMSE between reference and measured trajectory in synergistic motion were: F/E: 4.78°, R/U: 4.03°. The RMSE between reference and measured trajectory in F/E motion were: F/E: 3.62°, R/U: 0.53°. The RMSE between reference and measured trajectory in R/U motion were: F/E: 0.36°, R/U: 1.26°.

In the second experiment, we measured the actual torque output capability and human-machine interaction torque detection capability of HrWE by applying single axis (FE, RU, and PS) torque at the end-effector. When the torque increases by 0.5Nm, the displacement of the end-effector in the specified direction is recorded through the IMU and the interactive force is recorded through the three-dimensional force sensor. If the displacement of the end-effector in the specified direction exceeds 2°, we terminated the experiment and defined the applied torque as the actual output torque of HrWE. The experimental results are shown in Fig. 8. The maximum output torques of HrWE are 3.15Nm in F/E axis, 3.55Nm in R/U axis, and 2.74Nm in P/S axis. The RMSE between the reference interaction torques and measured interaction torques of HrWE are 0.092Nm in F/E axis, 0.025Nm in R/U axis, and 0.058Nm in P/S axis, respectively.

IV. Movement Intention Recognition

A. Decoding Algorithm

The spatial-temporal convolutional networks for gesture recognition (STCN-GR) proposed in our previous study [38] is used for movement intentions decoding. As shown in Fig. 9,

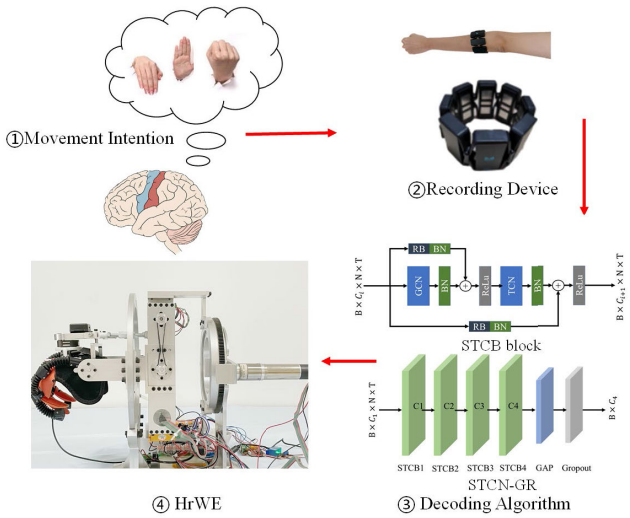

Fig. 9. The overview of the active rehabilitation training platform. The platform consists of the sEMG recording module, movement intention decoding module, and the HrWE.

the core structure of STCN-GR is the spatial-temporal convolution block which includes a graph convolution network (GCN) block and a temporal convolution network (TCN) block. Besides, batch normalization (BN) layers and ReLU layers are followed to speed up convergence and improve the expression ability of networks. Residual blocks (RBs) are used to stabilize the training, which uses 1×1 kernels to match input channels and out channels. The STCN-GR is stacked by M STCBs, in this work, $M = 4$. $c1$, $c2$, $c3$ and $c4$ denote the number of output channels of STCBs, which are set to 4, 6, 8, G (the number of gestures) respectively. A global average pooling (GAP) layer is added after the last STCB to improve generalization ability and get the final features, which

TABLE III
TABLE III RECOGNITION ACCURACY (%)

Subject	1	2	3	4	5	6	7	8	9	10	11
Session1	97.00	96.00	96.00	95.00	**98.00**	96.00	96.50	97.00	97.00	97.00	98.00
Session2	98.50	96.00	97.00	98.00	**98.50**	97.00	96.00	97.50	97.00	96.00	97.00
Average	97.75	96.00	96.50	96.50	**98.25**	96.50	96.25	97.25	97.00	96.50	97.50

replaces the full connection layer and reduces the number of parameters. Then, an optional dropout operation is performed.

B. Active Rehabilitation Platform Setup

The active rehabilitation platform is shown in Fig. 9. The MYO armband with 200Hz sampling rate is used for sEMG signals recording, which can record 8 channels sEMG signals simultaneously.

The decoding model should be trained before the active rehabilitation training. sEMG signal acquisition software will prompt the subjects to perform specific gestures, including hand open, fist, ulnar deviation, radial deviation, flexion, extension, pronation, supination and rest. The subject is asked to complete the prompt gesture within 5s. Each gesture will be repeated 10 times, and each repetition called a trial. A total of 90 trials are used to train the recognition model.

In the online experiment process, the offline training movement intention recognition model will be loaded first, then the screen will prompt users to perform specific wrist and hand movement (F/E, R/U, P/S, hand open/fist and rest). The subjects are required to try the relevant movement within 5s. Then, the recorded sEMG signals are fed into the model, and the decoded movement intentions are converted into control instruction to control the wrist exoskeleton.

We recruited 11 subjects for our experiments and each subject was asked to perform two session (200 trials of each session). The online recognition results are showed in TABLE III. It can be seen from TABLE III that the recognition accuracy is above 96%, and the highest is 98.25%.

V. DISCUSSION

In this paper, we propose a novel wrist exoskeleton HrWE. We first described the configuration of HrWE and analyzed the kinematics of HrWE. Then we evaluated the performance of HrWE. Finally, we designed an active rehabilitation paradigm based on surface EMG using HrWE.

In order to better develop the theory of hand function rehabilitation training based on the robotic strategy and reveal the mechanism of hand function rehabilitation, the exoskeletons should be able to assist the hand joint to the position where they can naturally reach. The existing wrist exoskeletons, or its RoM cannot encircle the PMS of wrist, or cannot provide enough DoF, or can't provide synergistic rehabilitation training of upper limb, fingers and wrist. The 3-DoF wrist exoskeleton HrWE proposed by us can provide sufficient output torque to drive the wrist to perform F/E, R/U and P/S movements (see Fig. 6). Specifically, in both uniaxial movement condition task and boundary elliptical movement condition task, the RoM of HrWE can almost encircle the PMS of wrist. In addition, this device can assist both left and right hands, and is suitable for individuals with arm length over 30cm and palm length of 8-12cm.

The core mechanism of HrWE is 2-RSS/RR configuration which is used to drive F/E and R/U joints. Moreover, the 2-RSS/RR configuration can be easily adapted to an upper limb exoskeleton proposed in our previous study [39] (see Fig. 1(d)) and provide hand rehabilitation module (see Fig. 1(c)). From Fig. 3 (c), it can be seen that the AWS of 2-RSS/RR will get larger as l_2 gets larger, while other link remain constant length. Based on the consideration of compact structure and user comfort, we finally set the length of $l2$ to 65mm, resulting in the AWS of 2-RSS/RR not fully covering the PMS of the wrist (see Fig. 5).

If only F/E and R/U movements are performed, the 2RSS/RR structure can be changed to an open type as in [28]. However, due to the structural characteristics of gears and bearings, it is difficult to design HrWE as an open type. In the future work, we will focus on optimizing the configuration of 2-RSS/RR and the driving structure of P/S joints to enhance the applicability of HrWE.

Current device can be fitted with handle or pneumatic glove at the end-effector (see Fig. 2(d) and Fig. 2(e)). The HrWE version with exoglove is more suitable for users whose hands can't grip the grip. In addition, the exoglove will not interfere with the device during movement within the AWS, so this will not affect the performance of HrWE. This article only provides a concept for retrofitting 2-RSS/RR into an upper limb rehabilitation robot. Due to the light weight (2.7kg) and low reflected inertia ($0.0012\text{kg}\cdot\text{m}^2$) of the 2-RSS/RR mechanism, it is theoretically feasible to be modified into the upper limb robot. In future work, we will focus on how to modify the 2-RSS/RR structure into the upper limb rehabilitation robot.

In our previous work, we have verified the feasibility of our proposed algorithm in gesture recognition [36]. In this paper, we combined the previous work, built a wrist active rehabilitation training platform based on sEMG signal. The results of experiments show that the proposed framework can be applied to active rehabilitation training. In patients with complete loss of hand function, sEMG signals can also be detected on the arm during hand movement attempts [40]. Therefore, the movement intention recognition strategy based on sEMG signals can be applied to patients' rehabilitation training earlier than the strategy based on force sensors. Although movement intention recognition based on invasive BCI can directly bypass the damaged central nervous system to control peripherals [41], this invasive approach is relatively poorly accepted by patients because of the need for surgery.

But stroke survivors typically have aberrant muscle activation patterns that may vary little from one task to the next. This paper only built a rehabilitation platform based on sEMG gesture recognition and HrWE, and in the future work, we will focus on applying this rehabilitation platform to clinical practice.

In this paper, the wrist exoskeleton designed based on the guidance of PMS was only evaluated from the mechanical properties, and the improvement of its rehabilitation effect was not verified by experiments. In addition, the human-computer interaction system should also be optimized based on clinical requirements.

VI. Conclusion

In this paper, we proposed a bioelectronic controlled hybrid serial-parallel wrist exoskeleton HrWE and analyzed its performance. The analysis results show that the HrWE has the following advantages:

(1) HrWE can assist patients to perform F/E, R/U and P/S movements individually or simultaneously. Specifically, both uniaxial movement and boundary elliptical movement can almost cover the PMS of wrist. This characteristic allows HrWE to better assist patients with rehabilitation training.

(2) The 2-RSS/RR configuration is lighter, and the structural parameters can be adjusted according to different design requirements. This characteristic allows the HrWE's end-effector to be fitted with the finger exoskeletons and the mechanism to be adapted into the upper limb exoskeletons. Moreover, HrWE is suit for both hands.

(3) Users can utilize the sEMG based rehabilitation paradigm to carry out robot-assist rehabilitation training. Moreover, the human-computer interaction system can make patients better participate in rehabilitation training.

In general, HrWE can further replace the work of therapists. Furthermore, the hand rehabilitation platform proposed by us is conducive to the optimization of the rehabilitation training paradigm, the development of hand rehabilitation theory and the exploration of rehabilitation mechanism.

References

[1] A. S. Go et al., "Heart disease and stroke statistics—2013 update: A report from the American Heart Association," *Circulation*, vol. 127, no. 1, pp. e6–e245, Apr. 2013.

[2] R. P. Van Peppen, G. Kwakkel, S. Wood-Dauphinee, H. J. Hendriks, P. J. Van der Wees, and J. Dekker, "The impact of physical therapy on functional outcomes after stroke: What's the evidence?" *Clin. Rehabil.*, vol. 18, no. 8, pp. 833–862, Dec. 2004.

[3] B. R. Brewer, S. K. McDowell, and L. C. Worthen-Chaudhari, "Post-stroke upper extremity rehabilitation: A review of robotic systems and clinical results," *Topics Stroke Rehabil.*, vol. 14, no. 6, pp. 22–44, Dec. 2007.

[4] L. E. Kahn, M. L. Zygman, W. Z. Rymer, and D. J. Reinkensmeyer, "Robot-assisted reaching exercise promotes arm movement recovery in chronic hemiparetic stroke: A randomized controlled pilot study," *J. NeuroEng. Rehabil.*, vol. 3, no. 1, p. 12, Jun. 2006.

[5] A. C. Lo et al., "Robot-assisted therapy for long-term upper-limb impairment after stroke," *New England J. Med.*, vol. 362, no. 19, pp. 1772–1783, May 2010.

[6] V. Klamroth-Marganska et al., "Three-dimensional, task-specific robot therapy of the arm after stroke: A multicentre, parallel-group randomised trial," *Lancet Neurol.*, vol. 13, no. 2, pp. 159–166, Feb. 2014.

[7] J. L. Patton, M. E. Stoykov, M. Kovic, and F. A. Mussa-Ivaldi, "Evaluation of robotic training forces that either enhance or reduce error in chronic hemiparetic stroke survivors," *Exp. Brain Res.*, vol. 168, no. 3, pp. 368–383, Jan. 2006.

[8] N. Hogan, H. I. Krebs, J. Charnnarong, P. Srikrishna, and A. Sharon, "MIT-MANUS: A workstation for manual therapy and training. I," in *Proc. IEEE Int. Workshop Robot Hum. Commun.*, Aug. 1992, pp. 161–165.

[9] H. Krebs, J. Celestino, D. J. Williams, M. Ferraro, B. Volpe, and N. Hogan, "A wrist extension for MIT-MANUS," *Adv. Rehabil. Robot*, vol. 306, pp. 377–390, Jan. 2004.

[10] M. J. Johnson, "Recent trends in robot-assisted therapy environments to improve real-life functional performance after stroke," *J. NeuroEng. Rehabil.*, vol. 3, no. 1, p. 29, Dec. 2006.

[11] C.-Y. Wu et al., "Effect of therapist-based versus robot-assisted bilateral arm training on motor control, functional performance, and quality of life after chronic stroke: A clinical trial," *Phys. Therapy*, vol. 92, no. 8, pp. 1006–1016, Jul. 2012.

[12] H. Thieme et al., "Mirror therapy for improving motor function after stroke: Update of a cochrane review," *Stroke*, vol. 50, no. 2, pp. e26–e27, Feb. 2019.

[13] P. W. Duncan et al., "Management of adult stroke rehabilitation care: A clinical practice guideline," *Stroke*, vol. 36, no. 9, pp. e100–e143, Sep. 2005.

[14] G. J. Kleinrensink et al., "Upper limb tension tests as tools in the diagnosis of nerve and plexus lesions," *Clin. Biomech.*, vol. 15, no. 1, pp. 9–14, Jan. 2000.

[15] G. A. Talebi, A. E. Oskouei, and S. K. Shakori, "Reliability of upper limb tension test 1 in normal subjects and patients with carpal tunnel syndrome," *J. Back Musculoskeletal Rehabil.*, vol. 25, no. 3, pp. 209–214, Aug. 2012.

[16] M. Pasquini et al., "Preclinical upper limb neurorobotic platform to assess, rehabilitate, and develop therapies," *Sci. Robot.*, vol. 7, no. 64, Mar. 2022, Art. no. eabk2378.

[17] M. van de Giessen et al., "A 4D statistical model of wrist bone motion patterns," *IEEE Trans. Med. Imag.*, vol. 31, no. 3, pp. 613–625, Mar. 2012.

[18] M. J. Rainbow, J. J. Crisco, D. C. Moore, and S. W. Wolfe, "Gender differences in capitate kinematics are eliminated after accounting for variation in carpal size," *J. Biomech. Eng.*, vol. 130, no. 4, Aug. 2008, Art. no. 041003.

[19] K. Nakamura, M. Beppu, R. M. Patterson, C. A. Hanson, P. J. Hume, and S. F. Viegas, "Motion analysis in two dimensions of radial-ulnar deviation of type I versus type II lunates," *J. Hand Surg.*, vol. 25, no. 5, pp. 877–888, Sep. 2000.

[20] S. Ueki et al., "Development of a hand-assist robot with multi-degrees-of-freedom for rehabilitation therapy," *IEEE/ASME Trans. Mechatronics*, vol. 17, no. 1, pp. 136–146, Feb. 2012.

[21] D. Buongiorno, E. Sotgiu, D. Leonardis, S. Marcheschi, M. Solazzi, and A. Frisoli, "WRES: A novel 3 DoF WRist ExoSkeleton with tendon-driven differential transmission for neuro-rehabilitation and teleoperation," *IEEE Robot. Autom. Lett.*, vol. 3, no. 3, pp. 2152–2159, Jul. 2018.

[22] L. Cappello, N. Elangovan, S. Contu, S. Khosravani, J. Konczak, and L. Masia, "Robot-aided assessment of wrist proprioception," *Frontiers Hum. Neurosci.*, vol. 9, p. 198, Apr. 2015.

[23] A. U. Pehlivan, F. Sergi, A. Erwin, N. Yozbatiran, G. E. Francisco, and M. K. O'Malley, "Design and validation of the RiceWrist-S exoskeleton for robotic rehabilitation after incomplete spinal cord injury," *Robotica*, vol. 32, no. 8, pp. 1415–1431, Jun. 2014.

[24] E. Pezent, C. G. Rose, A. D. Deshpande, and M. K. O'Malley, "Design and characterization of the OpenWrist: A robotic wrist exoskeleton for coordinated hand-wrist rehabilitation," in *Proc. Int. Conf. Rehabil. Robot. (ICORR)*, Jul. 2017, pp. 720–725.

[25] A. Gupta, M. K. O'Malley, V. Patoglu, and C. Burgar, "Design, control and performance of RiceWrist: A force feedback wrist exoskeleton for rehabilitation and training," *Int. J. Robot. Res.*, vol. 27, no. 2, pp. 233–251, Feb. 2008.

[26] Y. Wang and Q. Xu, "Design and testing of a soft parallel robot based on pneumatic artificial muscles for wrist rehabilitation," *Sci. Rep.*, vol. 11, no. 1, p. 1273, Jan. 2021.

[27] J. A. Martinez, P. Ng, S. Lu, M. S. Campagna, and O. Celik, "Design of wrist gimbal: A forearm and wrist exoskeleton for stroke rehabilitation," in *Proc. IEEE 13th Int. Conf. Rehabil. Robot. (ICORR)*, Jun. 2013, pp. 1–6.

[28] L. Zhang, J. Li, Y. Cui, M. Dong, B. Fang, and P. Zhang, "Design and performance analysis of a parallel wrist rehabilitation robot (PWRR)," *Robot. Auto. Syst.*, vol. 125, Mar. 2020, Art. no. 103390.

[29] P. Langhorne, F. Coupar, and A. Pollock, "Motor recovery after stroke: A systematic review," *Lancet Neurol.*, vol. 8, no. 8, pp. 741–754, Aug. 2009.

[30] H. Rodgers et al., "Robot assisted training for the upper limb after stroke (RATULS): A multicentre randomised controlled tria," *Lancet*, vol. 394, no. 10192, pp. 51–62, Jul. 2019.

[31] G. Kwakkel, B. J. Kollen, and H. I. Krebs, "Effects of robot-assisted therapy on upper limb recovery after stroke: A systematic review," *Neurorehabilitation Neural Repair*, vol. 22, no. 2, pp. 111–121, Mar. 2008.

[32] D. Borton, S. Micera, J. D. R. Millán, and G. Courtine, "Personalized neuroprosthetics," *Sci. Transl. Med.*, vol. 5, no. 210, Nov. 2013, Art. no. 210rv2.

[33] T. B. G. O. Dubbelink et al., "Wrist circumference-dependent upper limit of normal for the cross-sectional area is superior over a fixed cut-off value in confirming the clinical diagnosis of carpal tunnel syndrome," *Frontiers Neurol.*, vol. 12, Feb. 2021, Art. no. 625565.

[34] D. V. A. Mane, D. S. Satpute, and. D. A. Y. M., "Reconstruction of body height using right hand-palm length and middle finger length among Sangli district population," *Int. J. Res. Rev.*, vol. 9, no. 5, pp. 373–377, Jul. 2022.

[35] A. Mulu and B. Sisay, "Estimation of stature from arm span, arm length and tibial length among adolescents of aged 15–18 in Addis Ababa, Ethiopia," *Ethiop. J. Health Sci.*, vol. 31, no. 5, pp. 1053–1060, Sep. 2021.

[36] X. Kong and C. Gosselin, "Generation and forward displacement analysis of RPR-PR-RPR analytic planar parallel manipulators," *J. Mech. Des.*, vol. 124, no. 2, pp. 294–300, Jun. 2002.

[37] J. S. Dai, Z. Huang, and H. Lipkin, "Mobility of overconstrained parallel mechanisms," *J. Mech. Design*, vol. 128, no. 1, pp. 220–229, Jan. 2006.

[38] Z. P. Lai et al., "STCN-GR: Spatial–temporal convolutional networks for surface-electromyography-based gesture recognition," in *Proc. Int. Conf. Neural Inf. Process.*, 2021, pp. 27–39.

[39] H. Yan et al., "Configuration design of an upper limb rehabilitation robot with a generalized shoulder joint," *Appl. Sci.*, vol. 11, no. 5, p. 2080, Feb. 2021.

[40] J. E. Ting et al., "Sensing and decoding the neural drive to paralyzed muscles during attempted movements of a person with tetraplegia using a sleeve array," *J. Neurophysiol.*, vol. 126, no. 6, pp. 2104–2118, Dec. 2021.

[41] P. D. Ganzer et al., "Restoring the sense of touch using a sensorimotor demultiplexing neural interface," *Cell*, vol. 181, no. 4, pp. 763–773, May 2020.